

DRYLINE CHARACTERISTICS NEAR LUBBOCK, TEXAS, BASED ON RADAR AND
WEST TEXAS MESONET DATA FOR MAY 2005 AND MAY 2006

Bart Geerts¹

University of Wyoming

Submitted to *Weather and Forecasting*,
May 2007

¹ *Corresponding author address:* Bart Geerts, Department of Atmospheric Sciences, University of Wyoming, Laramie WY 82071, USA; email: geerts@uwyo.edu

Dryline characteristics near Lubbock, Texas, based on radar and West Texas Mesonet data for
May 2005 and May 2006

Abstract

Two months of Lubbock, Texas, radar reflectivity data and West Texas Mesonet data are examined to detect dryline fine-lines and to describe their thermodynamic and propagation characteristics. Before sunset the moist airmass east of the dryline was consistently denser than the dry airmass. This air density difference waned and even reversed after sunset, due to more rapid cooling on the dry side.

This study provides strong evidence that the formation and propagation of the dryline convergence zone is driven by the daytime air density difference, i.e. that the dryline behaves as a density current. The implication for forecasters is that the air density (or virtual potential temperature difference) across the dryline should be monitored, as a measure of dryline strength and as an additional indicator for the likelihood for convective initiation along the dryline.

1. Introduction

The dryline is a well-defined atmospheric boundary observed over the Southern Great Plains, between hot dry air to the west, and air of maritime tropical (mT) origin to the east. To a first order, the dryline can be considered as the intersection of the top of a capped boundary-layer containing the mT airmass and the sloping terrain east of the Rocky Mountains (e.g., Schaefer 1974). The dryline has clear diurnal characteristics and becomes more defined during the afternoon hours, when it tends to move eastward, at least in the absence of synoptic changes (Bluestein 1993, p284). The large-scale [$O(100 \text{ km})$] convergence along the dryline is attributed to the formation of a heat trough in the lee of the Rockies (e.g., McCarthy and Koch 1982; Parsons et al. 1991; Bluestein and Crawford 1997). The mature dryline is often a remarkably fine boundary [$O(1-10 \text{ km})$], with a substantial humidity jump and significant convergence over the depth of the convective boundary layer (Miao and Geerts 2007). On account of the fine-scale convergence, radars [including the Weather Surveillance Radar-88 Doppler (WSR-88D) radars] generally see the dryline as a reflectivity ‘fine-line’ (e.g., Wilson et al. 1992). The radar return is generally due to insects (Russell and Wilson 1997) that congregate in regions of convergent flow, apparently because they oppose the rising motion associated with the convergence (Geerts and Miao 2005). Satellite imagery is of little use, since the dryline is rarely marked by a cloud line or a cloud edge.

Forecasters’ interest in drylines is motivated mainly by the fact that drylines are “a major factor in the initiation of the severe thunderstorms in the central and southern United States during the spring” (Hane et al., 1993). Thus forecasters from southwest Texas to western Kansas routinely examine WSR-88D clear-air radar reflectivity surveillance scans for the presence of a

dryline fine-line. Clear-air echoes are limited to 70-100 km in the lowest elevation WSR-88D scan (0.5°), and the resulting radar coverage is rather limited, for instance in West Texas (**Fig. 1**).

The dryline tends to form on about 40% of the days, mainly in late spring (Bluestein 1993, p283), at an average longitude of 101°W (Hoch and Markowski 2005). This longitude is not covered well by the WSR-88D network in northwest Texas, since it falls between the AMA and LBB radars to the west and the FDR and DYX radars to the east (Fig. 1). While there is considerable day-to-day variability in dryline position due to synoptic conditions, on synoptically-quiescent days the dryline position remains relatively close to its climatological mean position. In recent years a dense network of automated weather stations has been installed in West Texas, the West Texas Mesonet (WTM, Schroeder et al. 2005). This allows a description of the airmass contrast across the dryline in unprecedented detail.

It has long been suggested that the fine-scale convergence leading to convective initiation, as well as the formation of a radar fine-line, is due to a difference in density in the adjacent air masses: in the afternoon the mT airmass may be cooler than the dry, hot air to the west of the dryline, and that drives an atmospheric density current similar to a sea breeze. Thus drylines have been labeled ‘inland sea breezes’ (Sun and Ogura 1979; Sun 1987; Bluestein and Crawford 1997). Sea breezes normally propagate inland, although their progression may be impeded by ambient offshore flow. Similarly, it depends on the ambient wind whether the dryline propagates westward (“retrogresses”). Retrogression does occur in many cases, mainly in the evening (Crawford and Bluestein 1997; Shaw et al. 1997).

Several detailed case studies have characterized the dryline as a density current (Bluestein et al. 1990; Parsons et al. 1991; Ziegler and Hane 1993; Hane et al. 1997; Atkins et al. 1998; Ziegler and Rasmussen 1998; Miao and Geerts 2007). On the other hand, Crawford and

Bluestein (1997) describe a retrogressing dryline without density current characteristics. Fine-scale convergence may be driven by other factors, e.g. differential vertical transfer of zonal momentum (Hane et al. 1997).

The purpose of this study is to use the dense WTM network to characterize drylines in the vicinity of the Lubbock WSR-88D radar, specifically to test the hypothesis that the dryline is the result of a density difference in adjacent airmasses. This study differs from previous ones in that it is not case-study based, but uses two months of data.

Data sources and analysis method are described in Section 2. Dryline characteristics are presented in Section 3, and the density current theory is discussed in Section 4.

2. Data sources and analysis method

Surveillance scan base reflectivity from the LBB WSR-88D radar data, obtained from the National Climatic Data Center (NCDC), and meteorological data from 18 WTM stations surrounding LBB were examined for two months, May 2005 and May 2006. The NCDC base reflectivity product generally came from the 0.5° elevation scan, although sometimes it came from a higher-elevation scan (1.3° or 1.5°), depending on the volume coverage pattern (VCP). Depending on storm development, the radar sometimes operated in VCPs other than the clear-air mode (VCP 31/32); in this case the fine-lines were still detectable, although less-well depicted.

The Integrated Data Viewer (IDV)² was used to display radar and station (**Fig. 2**). First, radar fine-lines were identified. Next, the humidity contrast revealed by the WTM data and synoptic analysis charts were used to confirm that they were drylines, and not cold fronts or thunderstorm outflow boundaries. Sixteen dryline days were identified in both months, i.e., 26% of the days. On one day two different, non-coincident drylines were encountered. Some dryline

² <http://www.unidata.ucar.edu/software/idv/>

fine-lines formed within the LBB domain, others moved into the area. Displays such as shown in Fig. 2 were then analyzed at 5 min intervals to determine the temperature, dewpoint, water vapor mixing ratio (r_v), and virtual potential temperature (θ_v) on opposite sides of the dryline. At each time, a pair of WTM stations was chosen, such that they were clearly located on either side of the radar fine-line, but not too far apart. The distance between suitable pairs averaged 57 km, ranging from 23 to 85 km.

The speed of the dryline fine-line normal to its orientation was computed using the LBB reflectivity maps at roughly hourly intervals and the ‘range and bearing’ tool in IDV. The dryline orientation was determined at the same intervals by drawing a best-fit line through the fine-line. Most fine-lines could be detected to a radar range of 80-100 km for VCP 31/32. The 11 May 2005 dryline was detectable out to 110 km (Fig. 2). We found that in most cases the fine-line had to be within ~60 km of LBB for its orientation and speed to be determinable.

LBB reflectivity maps were examined for the period 18 UTC- 6 UTC (noon to midnight CST) on each of the 62 days. These maps were missing for variable periods of time on several days, including on some dryline days. Thus it is possible that some drylines were missed. Since this study focuses on the fine-scale thermodynamic properties of the dryline, the presence of a radar fine-line is deemed essential. Thus the periods without LBB radar data were excluded from the dataset to be examined in this study. One exception is the 2 May 2006 dryline, for which LBB radar data were available only between 0000-0112 UTC (on 3 May), that is a fraction of the dryline lifetime. The exception was made because this was the most intense of all cases, and because the location and propagation of this dryline at radar-data-void times could be estimated from the WTM data: the clear dryline passage allowed us to manually map the estimated dryline positions at various times, from which the speed and orientation were inferred.

The difference in air density ρ between stations ($\Delta\rho$) is expressed as a θ_v difference ($\Delta\theta_v$) as follows. Assuming that the differences are much smaller than the mean values (written with over-bars), and assuming that relative pressure differences are small, the ideal gas law implies that

$$\frac{\Delta\rho}{\bar{\rho}} = -\frac{\Delta\theta_v}{\bar{\theta}_v} \cong -\frac{\Delta\theta}{\bar{\theta}} - 0.61\Delta r_v \quad (1)$$

As will be shown in Section 3, typical near-dryline measurements during the afternoon indicate that the mT airmass has a lower θ_v value, compared to the west side of the dryline, and thus a higher air density. This density difference is driven by temperature (the mT airmass is cooler), but it is smaller than due the temperature difference alone [first term on the right side of (1)], because the temperature effect is partially offset by the humidity difference across the dryline [second term on the right side of (1)]. Moist air is lighter than dry air at the same temperature and pressure, but it takes a 5-6 g/kg mixing ratio difference to offset a 1K potential temperature difference. The average Δr_v for the 17 drylines in this study was 4.1 g/kg. The average $\Delta\theta$ was -2.4 K, and the average $\Delta\theta_v$ was -1.6K³. These averages exclude the cases with a reverse temperature difference (cooler air on the west side), discussed below.

3. Results

a. General dryline characteristics

We examine the humidity and density contrast, as well as the propagation properties, for the 17 drylines in this study. A variety of dryline fine-lines were observed; some were straight (as in Fig. 2) or arc-shaped, others were more sinuous. The most frequent mean orientation of

³ We define the difference between airmasses as [moist side value]-[dry side value]. Thus Δr_v is strictly positive, but $\Delta\theta_v$ can be of either sign.

the fine-lines was NNE-SSW (**Fig. 3**), specifically between 10° and 40° from north. The histogram in Fig. 3 reveals a secondary peak, with a NW-SE orientation (-45°). These fine-lines were generally located to the NE of LBB. This anomalous local orientation may partly be attributable to the NNW-SSE orientation of the Caprock Escarpment between the latitudes of LBB and AMA. Because most drylines are roughly N-S oriented, we simply refer to the propagation as eastward (positive) or westward (negative). More precisely, a positive propagation speed is eastward or northward, by definition.

One particularly vigorous dryline occurred on 2 May 2006 (**Fig. 4**). The dryline was located in a synoptic-scale trough from northern Mexico to West Kansas (**Fig. 5**), and was associated with strong confluence on the synoptic scale and in the vicinity of LBB (Fig. 4). Before 22 UTC the dryline slowly propagated eastward, and after 22 UTC it propagated westward, eventually reaching a speed of 8.3 ms^{-1} . The station data indicate that it remained within the domain of interest for 6.5 hours. Several thunderstorms formed just east of this dryline (Fig. 4), some severe, including one tornadic storm at 2240 UTC at 130 km to the northeast of LBB, and later in the evening a severe squall line formed further east.

In neither panel of Fig. 4, the LBB radar was in clear-air VCP, because of the storms to the east. Because of the higher base elevation angle (1.3°) for this VCP, the maximum range at which the fine-line can be seen is less than in Fig. 2. The passage of the retrogressive dryline at station XSLS between 00 and 01 UTC is obvious in Fig. 4: the temperature dropped from 92 to 79 °F, the dewpoint increased from 23 to 53 °F, and the wind switched from 10 kts from 260° to 25 kts from 150°. The XSLS station pressure rose by 2.6 hPa (not shown). For all these variables, most of the change was concentrated between 0020 and 0025 UTC. Such rapid

changes were used to pinpoint the location of the dryline at times that radar data were not available on this day.

With the exception of a few cases, the virtual potential temperature was lower in the mT airmass for all 17 drylines, at any time before sunset (**Fig. 6**). The θ_v deficit was as large as 8.4 K on 2 May 2006, just after 00 UTC (6 pm CST) (**Fig. 7**), but peak $\Delta\theta_v$ values for other drylines were only half as large. The mixing ratio difference was large on 2 May 2006 (4-8 g kg⁻¹), but larger differences were observed for two other drylines (Fig. 6). In terms of the θ_v gradient instead of the θ_v difference, the 2 May 2006 case stands out even more (not shown). It is possible that on 2 May 2006 the mT airmass was cooled by outflows from the thunderstorms to the east. The first ones formed around 20 UTC, but precipitation may have been present at an earlier time. This cooling appears to have been widespread; during the short period with radar data on that day, we did not see any outflow boundaries approaching the dryline from the east.

Generally the drylines with a larger humidity contrast also had a larger $\Delta\theta_v$ (Fig. 6), i.e. they were more baroclinic. Drylines with a larger Δr_v and larger $\Delta\theta_v$ tended to be associated with more confluent flow, and better-defined radar fine-lines; we did not quantify these relationships.

b. Dryline baroclinicity

The θ_v deficit on the moist side of the 17 drylines in this study generally increased slightly with time until ~6 pm CST (00 UTC), and it vanished suddenly near sunset (Fig. 7). This applies also for the 2 May 2006 dryline. Three drylines were observed in the LBB coverage area well after sunset. In each of these cases, a θ_v deficit developed on the *dry* side, with a magnitude of up to 6 K. This reversal is due to more rapid evening cooling on the dry side than in the mT airmass, in each of the three cases. The evolution of Δr_v for all 17 drylines indicates

that the humidity contrast did not change much around sunset (**Fig. 8**). The humidity contrast tends to be largest in the late afternoon (6 pm CST), at the time that the radar fine-line is best-defined, and the fine-scale convergence strongest. The evening decrease of the humidity contrast is rather gradual.

The gradual increase in $\Delta\theta_v$ towards 00 UTC has been documented before for select dryline case studies using detailed aircraft data [see Figs. 13 and 14 in Miao and Geerts (2007)]. To our knowledge the rapid decrease of $\Delta\theta_v$ after 00 UTC, and its sign reversal after sunset, has not been documented. Several case studies have mentioned a θ_v deficit on the moist side of the dryline (NSSP Staff 1963; Bluestein et al. 1990; Parsons et al. 1991; Ziegler and Hane 1993; Hane et al. 1997; Atkins et al. 1998; Ziegler and Rasmussen 1998), but all these observations were taken between ~21-01 UTC, i.e. before sunset. One exception can be found in Crawford and Bluestein (1997): their Fig. 13 describes a west-bound (retrogressing) dryline passage at 0140 UTC on 12 May 1991, about the time of sunset. This passage was marked by a 1.5 K $\Delta\theta_v$ *increase*, implying that the moist side had a higher θ_v .

c. Dryline baroclinicity and propagation

It is well-known that under synoptically-quiet conditions the dryline tends to move eastward during the daytime and westward in the late afternoon and evening (e.g., Bluestein 1993, p284; Crawford and Bluestein 1997). The 17 drylines in this study confirm this tendency (**Fig. 9**). There is much scatter though, possibly because we did not attempt to isolate the fair-weather drylines from the total sample. (The number of points in Fig. 9 is much lower than in previous figures because the dryline fine-line displacement could only reliably be determined at

hourly intervals.) The 2 May 2006 also shows this reversal in dryline motion, at the relatively early time of 330 pm CST.

To test whether drylines behave as density current, we estimate the ‘relative’ dryline propagation speed (U_{rel}), i.e. relative to the mean wind (U_{env}) in the dryline vicinity. U_{env} is assumed to be the average wind at the 18 WTM stations used in this study. The component of that mean wind normal to the dryline is subtracted from the fixed-frame dryline propagation speed U_{fix} , i.e. $U_{rel} = U_{fix} - U_{env}$. Laboratory experiments (summarized in Simpson 1999) suggest that the speed of a density current (U_{dc}) can be estimated as follows:

$$U_{dc} = K \sqrt{\frac{gD\Delta\theta_v}{\bar{\theta}_v}} \quad (2)$$

Here g is the gravitational acceleration, D is the depth of the density current (m) and K is a constant; experimental values for K for atmospheric density currents range between 0.7-1.0 (e.g., Wakimoto 1982; Mueller and Carbone 1987; Kingsmill and Crook 2003). We use a value $K=0.7$. Some form of (2) is commonly encountered in the literature, including in atmospheric applications. Equation (2) assumes that there is no mean flow. The effective density current speed ($U_{dc,fix}$) can be assumed to be the speed of the current embedded in the ambient flow, $U_{dc,fix}=U_{dc}+U_{env}$. This assumes that the flow is Galilean invariant (Kingsmill and Crook 2003). Based on laboratory observations, Simpson and Britter (1980) proposed an effective speed of $U_{dc,fix}=U_{dc}+0.7U_{env}$. This reduction accounts for the effects of surface friction.

The observed relative propagation speed U_{rel} of the 17 drylines in this study is plotted against $\Delta\theta_v$ in **Fig. 10**. Negative values of U_{rel} indicate westward (or southward) motion relative to the ambient flow. Also shown is the dependence of U_{dc} on $\Delta\theta_v$, according to (2), assuming $K=0.7$ and $D=1000$ m. During the daytime $|U_{rel}|$ increases with $|\Delta\theta_v|$, and the increment in $|\Delta\theta_v|$

on the ordinate for a given $|U_{rel}|$ increment on the abscissa increases with $|\Delta\theta_v|$, i.e. the relationship is not linear, consistent with (2). So the relationship between the observed relative dryline propagation speed and $\Delta\theta_v$ is indicative of density current behavior, but for a given $\Delta\theta_v$, the observed speed is generally lower than the theoretical value. Computing the relative propagation speed as $U_{rel} = U_{fix} - 0.7U_{env}$, as in Simpson and Britter (1980), does not substantially improve the match between observations and the theoretical estimate in Fig. 10 (not shown). The least-square-fit quadratic equation for all points with $\Delta\theta_v < 0$ in Fig. 10,

$$\Delta\theta_v = a + bU_{dc}^2$$

(with a and b constants derived from a regression) gives a value for $a = -0.019$ K and $b = 0.098$ $\text{K s}^2 \text{m}^{-2}$, from which one obtains $K = 0.57$, still assuming $D = 1000$ m. The density current depth (or depth of the mT airmass) is unknown; it may be shallower than 1000 m, esp. during the retrogressive stage (Atkins et al. 1998). In any event, the relationship between the relative dryline propagation speed and $\Delta\theta_v$ shown in Fig. 10, before sunset, is a strong confirmation of relevance of density current dynamics.

After sunset no such relationship between U_{rel} and $\Delta\theta_v$ is apparent in Fig. 10: there is no evidence for an increase in positive (eastbound) U_{rel} as $\Delta\theta_v$ increases. In many cases U_{rel} is still negative (westbound). We interpret this motion as due to momentum inertia, given the rapid reversal of the sign of $\Delta\theta_v$ near sunset: initially, some drylines still propagate westward relative to the mean flow, but later their relative motion vanishes or reverses.

4. Discussion

The analysis of this relatively small sample of drylines convincingly demonstrates that (a) the mT airmass is generally denser than the dry airmass during the formation and mature stages

of the dryline; and (b) the formation of a dryline fine-line convergence zone and its propagation are consistent with density current theory. A number of case studies have confirmed these two conclusions (Bluestein et al. 1990; Parsons et al. 1991; Ziegler and Hane 1993; Hane et al. 1997; Atkins et al. 1998; Ziegler and Rasmussen 1998; Miao and Geerts 2007), but to our knowledge this has not been demonstrated with a two-month sample of operational data in West Texas. A study of this kind has only become possible in recent years because of the WTM.

One finding not revealed by previous case studies regards the rapid decrease and sign reversal of the density difference $\Delta\theta_v$ across the dryline near sunset (Fig. 7). As mentioned in Section 3b, this change is largely due to the more rapid evening cooling on the dry side, compared to the moist side of the dryline. This must relate to the surface heat balance, specifically the greater net longwave radiation loss in the evening on the dry side, on account of the lower atmospheric water vapor content. Similarly, the build-up of $\Delta\theta_v$ during the afternoon (with cooler air on the moist side) probably relates to differences in surface heat balance, in particular the dominance of latent heat flux over sensible heat flux on the moist side, and the dominance of sensible over latent heat flux on the dry side of the developing dryline. This will be examined in detail in a proposed field campaign, Simultaneous Observation of the Near-Dryline Environment, SONDE-08.

Retrogression commonly occurs, especially in the mature and decaying stages of the dryline (Fig. 9), in fact in all but two of the drylines in this study. (Both of these exceptions are marked by an approaching cold front.) The question may be asked how, in the absence of synoptic flow, a density (or gravity) current can travel uphill, westward up the slope of the Great Plains. That terrain slope α is about 100 m per 100 km, or $|\tan\alpha|\sim 10^{-3}$. The horizontal (terrain-

following) surface pressure gradient force PGF induced by density differences is [based on Mahrt (1982) and applied to the dryline situation]:

$$PGF = \frac{g\Delta\theta_v}{\theta_v} \sin \alpha + \frac{g}{\theta_v} \frac{\partial(D\theta_v)}{\partial x} \cos \alpha \quad (3)$$

This PGF drives the zonal flow u ($Du/Dt = PGF$). There may be other forces, such as the Coriolis force, friction, and the regional PGF that is not a hydrostatic product of $\Delta\theta_v$ in the boundary-layer; these are ignored, for simplicity. Mahrt (1982) developed the gravity flow equations for downslope (drainage) flow but it can be applied to local *upslope* flow as well. The first term in (3) drives a layer of denser air on the sloping Great Plains eastward ($\Delta\theta_v < 0$, $\sin\alpha < 0 \rightarrow PGF > 0$, $Du/Dt > 0$), until the isentropes are level ($\Delta\theta_v = 0$). The second term in (3) is a hydrostatic pressure gradient: it is due to the higher weight of the denser fluid over a depth D . It allows for westward (upslope) acceleration if denser air occurs to the east ($\partial\theta_v/\partial x < 0$, $\cos\alpha > 0 \rightarrow Du/Dt < 0$), assuming D is constant. For the typical slope of the Great Plains, we can then write (3) as:

$$PGF = \frac{g}{\theta_v} \left(10^{-3} \Delta\theta_v + D_{dc} \frac{\partial\theta_v}{\partial x} \right) \quad (4)$$

For a $\Delta\theta_v$ of 2 K over $\Delta x = 20$ km (typical values found in this study), and again $D = 1000$ m, the first term between the brackets in (4) is 100 times smaller than the second. Thus upslope gravity flow ($Du/Dt < 0$) is possible, but limited of course to the point where the θ_v contours become level.

The dryline retrogression speed does seem to wane somewhat after sunset, according to Fig. 9. Two mechanisms for the termination of westbound propagation may occur. Firstly, if $\Delta\theta_v$ does not change, the slope of the terrain imposes a limit, as discussed above. Secondly, $\Delta\theta_v$

does change in reality (Fig. 7), and this is sufficient to stall the westward propagation and initiate eastbound katabatic flow.

5. Conclusion

Reflectivity imagery from the Lubbock, Texas, WSR-88D radar and West Texas Mesonet station data were used to detect and describe drylines in the months of May 2005 and May 2006.

17 drylines were detected, on 16 days. The key findings are as follows.

- (a) The moist airmass east of the dryline was consistently denser than the dry airmass during the formation and mature stages of the dryline; typical differences in virtual potential temperature across the dryline ($\Delta\theta_v$) are 2-3 K over a distance of ~50 km.
- (b) This density difference peaked in the late afternoon and rapidly weakened, and even reversed, around sunset. This weakening and reversal is attributed to more rapid evening cooling on the dry side, presumably due to the greater longwave radiation loss at the surface there.
- (c) The formation of a dryline convergence zone and a radar fine-line, as well as the propagation of the dryline, are consistent with density current theory. According to this theory, the convergence and uplift along the dryline are stronger when $\Delta\theta_v$ is larger. Thus, *ceteris paribus*, the potential for lifted air to reach the level of free convection increases with $\Delta\theta_v$. Therefore, forecasters trying to determine dryline ‘strength’ and likelihood of convective initiation along the dryline are encouraged to monitor the observed or modeled $\Delta\theta_v$ in West Texas, in addition to currently-used indicators, such as convective inhibition.

Acknowledgements: This work was supported by a grant from the National Science Foundation.
The data were collected by Kyle D. Wright as part of his undergraduate senior research project.

References

- Atkins, N.T., R. M. Wakimoto, and C. L. Ziegler, 1998: Observations of the finescale structure of a dryline during VORTEX 95. *Mon. Wea. Rev.*, **126**, 525–550.
- Bluestein, H.B., 1993: *Synoptic-dynamic meteorology in midlatitudes, Vol II: Observations and theory of weather systems*. Oxford University Press, 594pp.
- _____, E.W. McCaul Jr., G.P. Byrd, R.L. Walko and R. Davies-Jones, 1990: An observational study of splitting convective clouds. *Mon. Wea. Rev.*, **118**, 1359–1370.
- _____, and T. M. Crawford, 1997: Mesoscale dynamics of the near-dryline environment: analysis of data from COPS-91. *Mon. Wea. Rev.*, **125**, 2161–2175.
- Crawford, T.M., and H.B. Bluestein, 1997: Characteristics of a dryline passage during COPS-91. *Mon. Wea. Rev.*, **125**, 463–477.
- Geerts, B., and Q. Miao, 2005: The use of millimeter Doppler radar echoes to estimate vertical air velocities in the fair-weather convective boundary layer. *J. Atmos. Ocean. Tech.*, **22**, 225–246.
- Hane, C.E., C.L. Ziegler, and H.B. Bluestein, 1993: Investigation of the dryline and convective storms initiated along the dryline: field experiments during COPS–91. *Bull. Amer. Meteor. Soc.*, **74**, 2133–2145.
- _____, H.B. Bluestein, T.M. Crawford, M.E. Baldwin, and R.M. Rabin, 1997: Severe thunderstorm development in relation to along-dryline variability: a case study. *Mon. Wea. Rev.*, **125**, 231–251.
- Hoch, J., and P. Markowski, 2005: Climatology of springtime dryline position in the U.S. Great Plains region. *J. Climate*, **18**, 2132–2137.

- Kingsmill, D. E., and N. A. Crook, 2003: An observational study of atmospheric bore formation from colliding density currents. *Mon. Wea. Rev.*, **131**, 2985–3002.
- Mahrt, L., 1982: Momentum balance of gravity flows. *J. Atmos. Sci.*, **39**, 2701–2711.
- McCarthy, J., and S.E. Koch, 1982: The evolution of an Oklahoma dryline. Part I: A meso- and subsynoptic-scale analysis. *J. Atmos. Sci.*, **39**, 225–236.
- Miao, Q., and B. Geerts, 2007: Fine-scale vertical structure and dynamics of some dryline boundaries observed in IHOP. *Mon. Wea. Rev.*, in press.
- Mueller, C. K., and R.E. Carbone, 1987: Dynamics of a thunderstorm outflow. *J. Atmos. Sci.*, **44**, 1879–1898.
- NSSP Staff, 1963: Environmental and thunderstorm structures as shown by National Severe Storms Project observations in spring 1960 and 1961. *Mon. Wea. Rev.*, **91**, 271–292.
- Parsons, D., M. A. Shapiro, R. M. Hardesty, R. J. Zamora, and J. M. Intrieri, 1991: The finescale structure of a West Texas dryline. *Mon. Wea. Rev.*, **119**, 1242–1258.
- Russell, R.W., and J.W. Wilson, 1997: Radar-observed “fine lines” in the optically clear boundary layer. Reflectivity contributions from aerial plankton and its predators. *Boundary Layer Meteor.*, **82**, 235–262.
- Schaefer, J.T., 1974: The life cycle of the dryline. *J. Appl. Meteor.*, **13**, 444–449.
- Schroeder, J.L., W.S. Burgett, K.B. Haynie, I. Sonmez, G.D. Skwira, A.L. Doggett, and J.W. Lipe, 2005: The West Texas Mesonet: a technical overview. *J. Atmos. Oceanic Technol.*, **22**, 211–222.
- Shaw, B. L., R.A. Pielke, and C.L. Ziegler, 1997: A three-dimensional numerical simulation of a Great Plains dryline. *Mon. Wea. Rev.*, **125**, 1489–1506.

- Simpson, J.E., 1999: *Gravity Currents in the Environment and the Laboratory*. Cambridge University Press, 2nd edition, 258 pp.
- _____, and R. E. Britter, 1980: A laboratory model of an atmospheric mesofront. *Quart. J. Roy. Meteor. Soc.*, **106**, 485–500.
- Sun, W.-Y., 1987: Mesoscale convection along the dryline. *J. Atmos. Sci.*, **44**, 1394–1403.
- _____, and Y. Ogura, 1979: Boundary layer forcing as a possible trigger to squall line formation. *J. Atmos. Sci.*, **36**, 235–254.
- Wakimoto, R. M., 1982: The life cycle of thunderstorm gust fronts as viewed with Doppler radar and rawinsonde data. *Mon. Wea. Rev.*, **110**, 1060–1082.
- Wilson, J.W., G.B. Foote, N.A. Crook, J.C. Fankhauser, C.G. Wade, J.D. Tuttle, and C.K. Mueller, 1992: The role of boundary layer convergence zones and horizontal rolls in the initiation of thunderstorms: a case study. *Mon. Wea. Rev.*, **120**, 1785-1815.
- Ziegler, C.L., and C.E. Hane, 1993: An observational study of the dryline. *Mon. Wea. Rev.*, **121**, 1134–1151.
- _____, and E.N. Rasmussen, 1998: The initiation of moist convection at the dryline: forecasting issues from a case study perspective. *Wea. Forecasting*, **13**, 1106–1131.

FIGURE CAPTIONS

Fig. 1: Map of WSR-88D radars and highways in West-Texas. The grey circles, with a radius of 70 km, represent the typical clear-air coverage of the boundary layer. The preferred longitude of drylines at 00 UTC is based on the dryline climatology by Hoch and Markowski (2005).

AMA=Amarillo; DYX=Dyess Air Force Base; FDR= Frederick, Oklahoma; LBB=Lubbock; MAF= Midland/ Odessa; SJT= San Angelo.

Fig. 2: Example of a dryline fine-line and WTM station observations at 2340 UTC on 11 May 2005. The color field (with key bar on the left) is the 0.5° elevation base reflectivity (dBZ) from LBB. The conventional part of the station data are the winds (kts), the temperature (°F), and the dewpoint (°F). The unconventional numbers are virtual potential temperature (upper right, units K) and mixing ratio (lower right, units $g\ kg^{-1}$). The station ID is shown below the station. The scale can be inferred from the range rings, shown at 40 km intervals. The red lines are county borders.

Fig. 3: Histogram of dryline orientations near LBB. A north-south orientation is 0°.

Fig. 4: As Fig. 2, but illustrating the vigorous 2 May 2006 dryline at (a) 0000 UTC and (b) 0100 UTC on 2006-05-03.

Fig. 5: Synoptic situation of the 2 May 2006 dryline.

Fig. 6: Scatterplot of the difference in mixing ratio versus the difference in virtual potential temperature, between stations on opposite side of the dryline, at any time before sunset. The linear regression line is shown as well. The circled points apply to the 2 May 2006 dryline.

Fig. 7: Trend of $\Delta\theta_v$ across the drylines (CST=UTC-6). The circled points apply to the 2 May 2006 dryline. The times of solar noon and sunset (on 1 May and 31 May) in Lubbock, Texas, are indicated.

Fig. 8: As Fig. 7, but for the humidity difference Δr_v .

Fig. 9: Trend of the propagation speed of the dryline fine-line. The circled points apply to the 2 May 2006 dryline.

Fig. 10: Scatterplot of the dryline propagation speed relative to the ambient flow (U_{rel}) against $\Delta\theta_v$. Also shown are a theoretical dependence of density current speed on $\Delta\theta_v$, and the least-square fit for the points with $\Delta\theta_v < 0$.

Figures

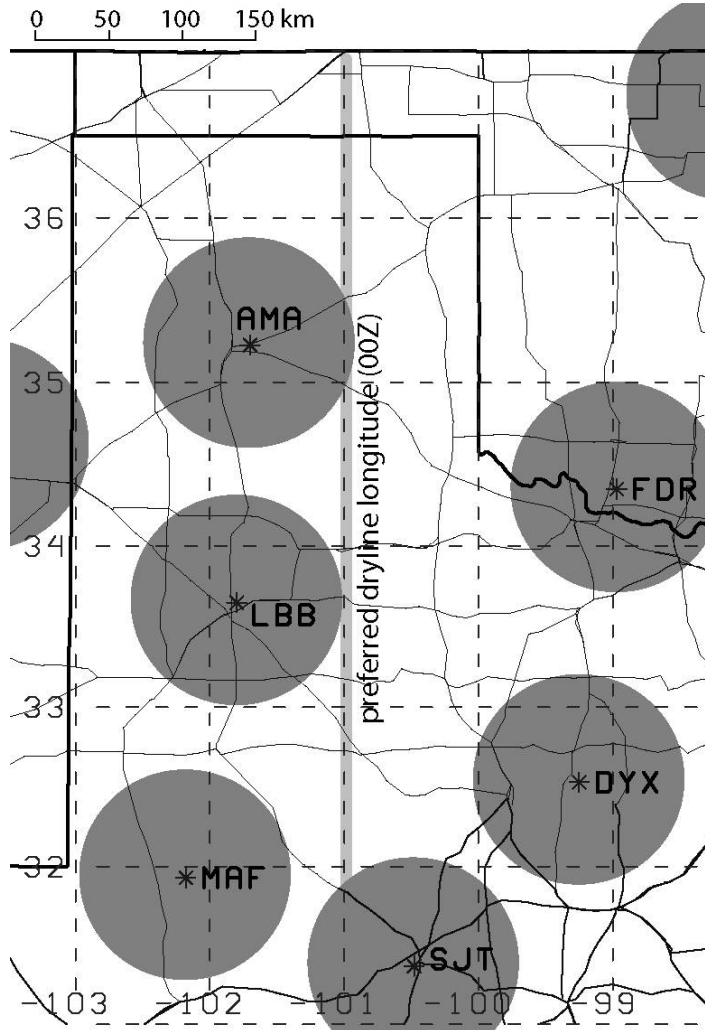


Fig. 1: Map of WSR-88D radars and highways in West-Texas. The grey circles, with a radius of 70 km, represent the typical clear-air coverage of the boundary layer. The preferred longitude of drylines at 00 UTC is based on the dryline climatology by Hoch and Markowski (2005). AMA=Amarillo; DYX=Dyess Air Force Base; FDR= Frederick, Oklahoma; LBB=Lubbock; MAF= Midland/ Odessa; SJT= San Angelo.

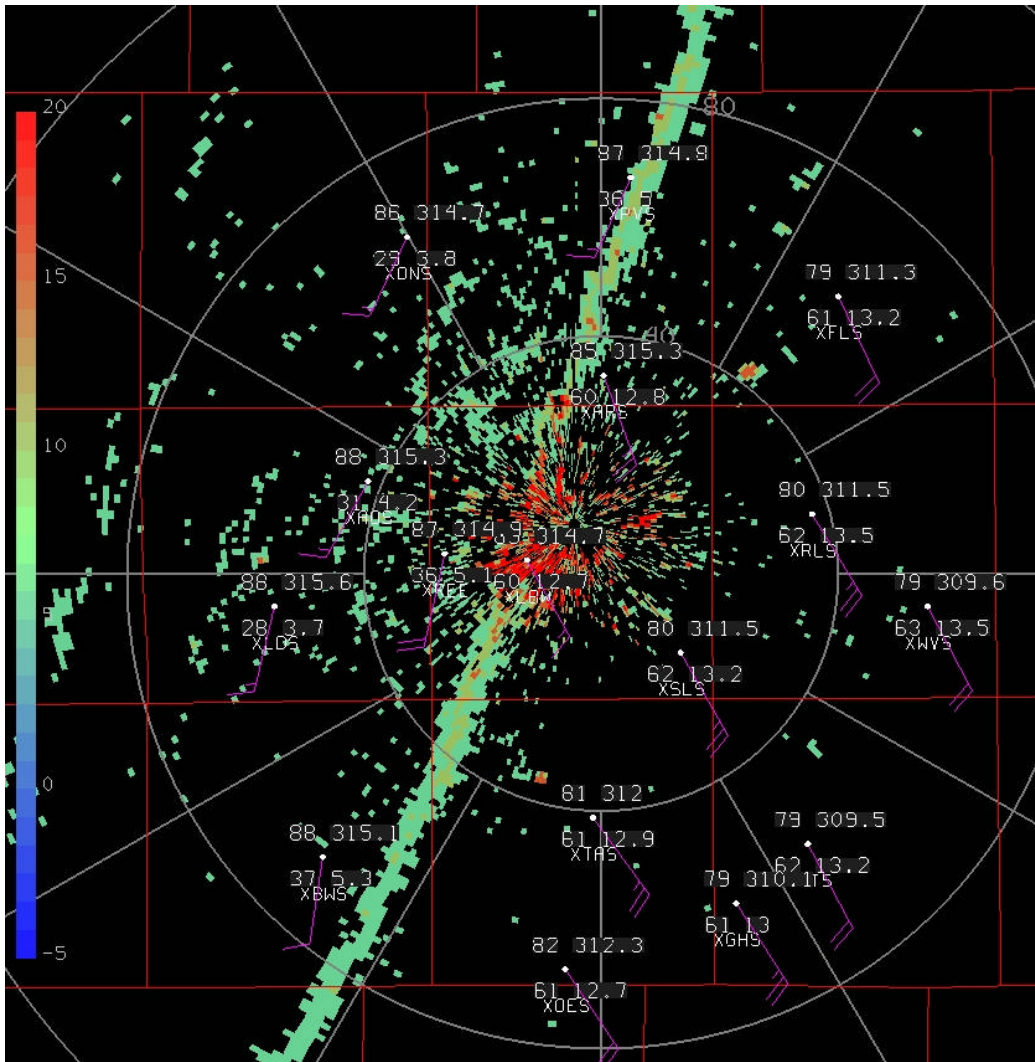


Fig. 2: Example of a dryline fine-line and WTM station observations at 2340 UTC on 11 May 2005. The color field (with key bar on the left) is the 0.5° elevation base reflectivity (dBZ) from LBB. The conventional part of the station data are the winds (kts), the temperature (°F), and the dewpoint (°F). The unconventional numbers are virtual potential temperature (upper right, units K) and mixing ratio (lower right, units g kg^{-1}). The station ID is shown below the station. The scale can be inferred from the range rings, shown at 40 km intervals. The red lines are county borders.

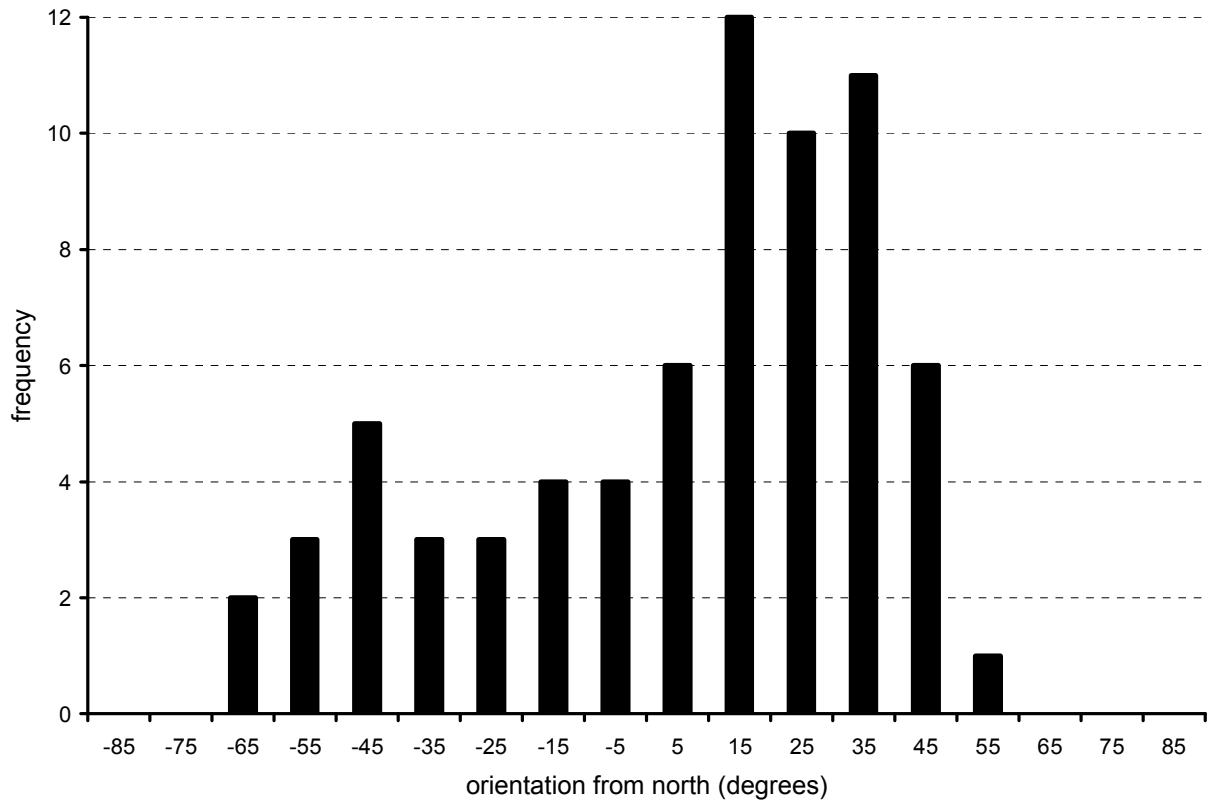


Fig. 3: Histogram of dryline orientations near LBB. A north-south orientation is 0°.

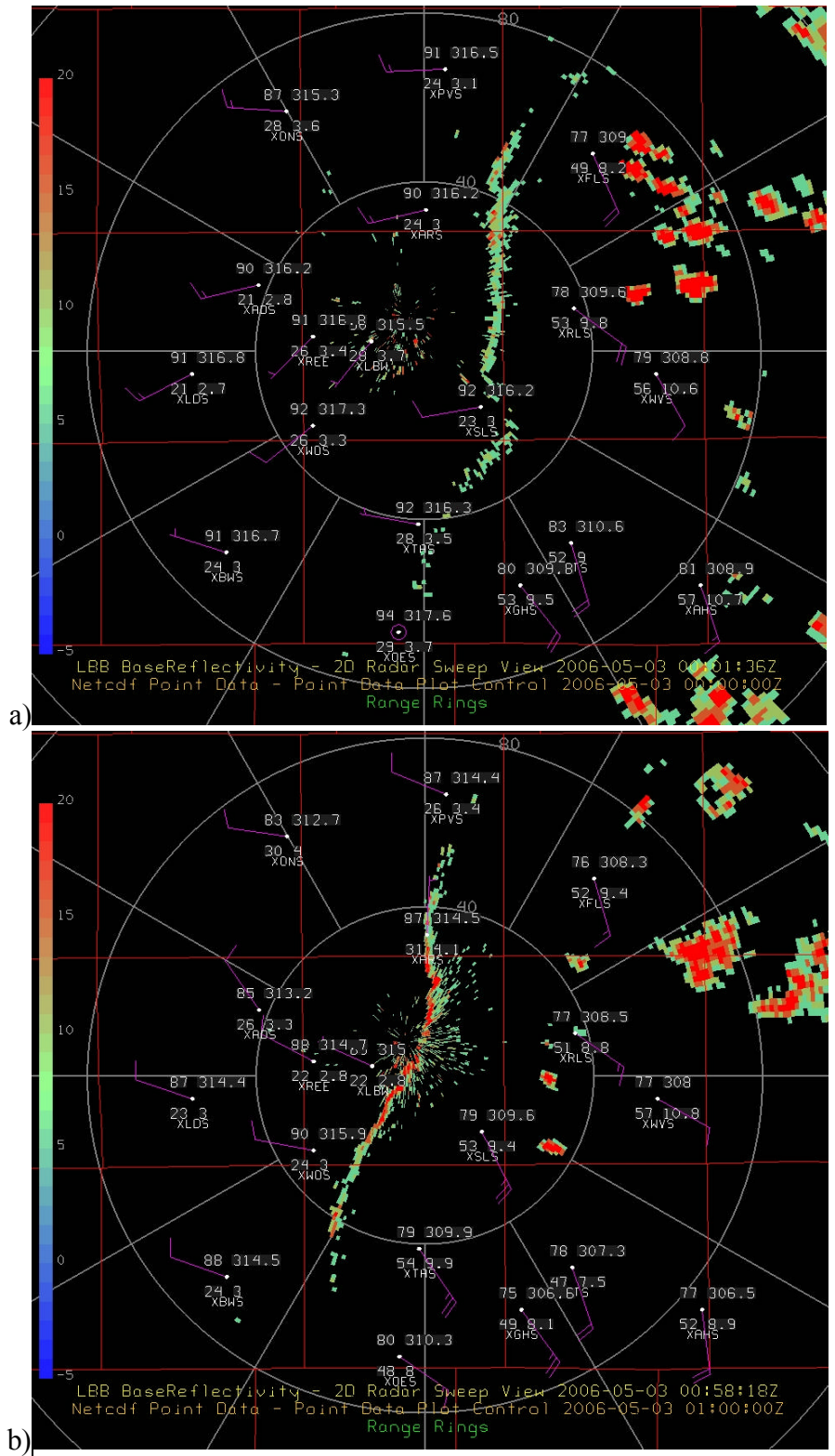


Fig. 4: As Fig. 2, but illustrating the vigorous 2 May 2006 dryline at (a) 0000 UTC and (b) 0100 UTC on 2006-05-03.

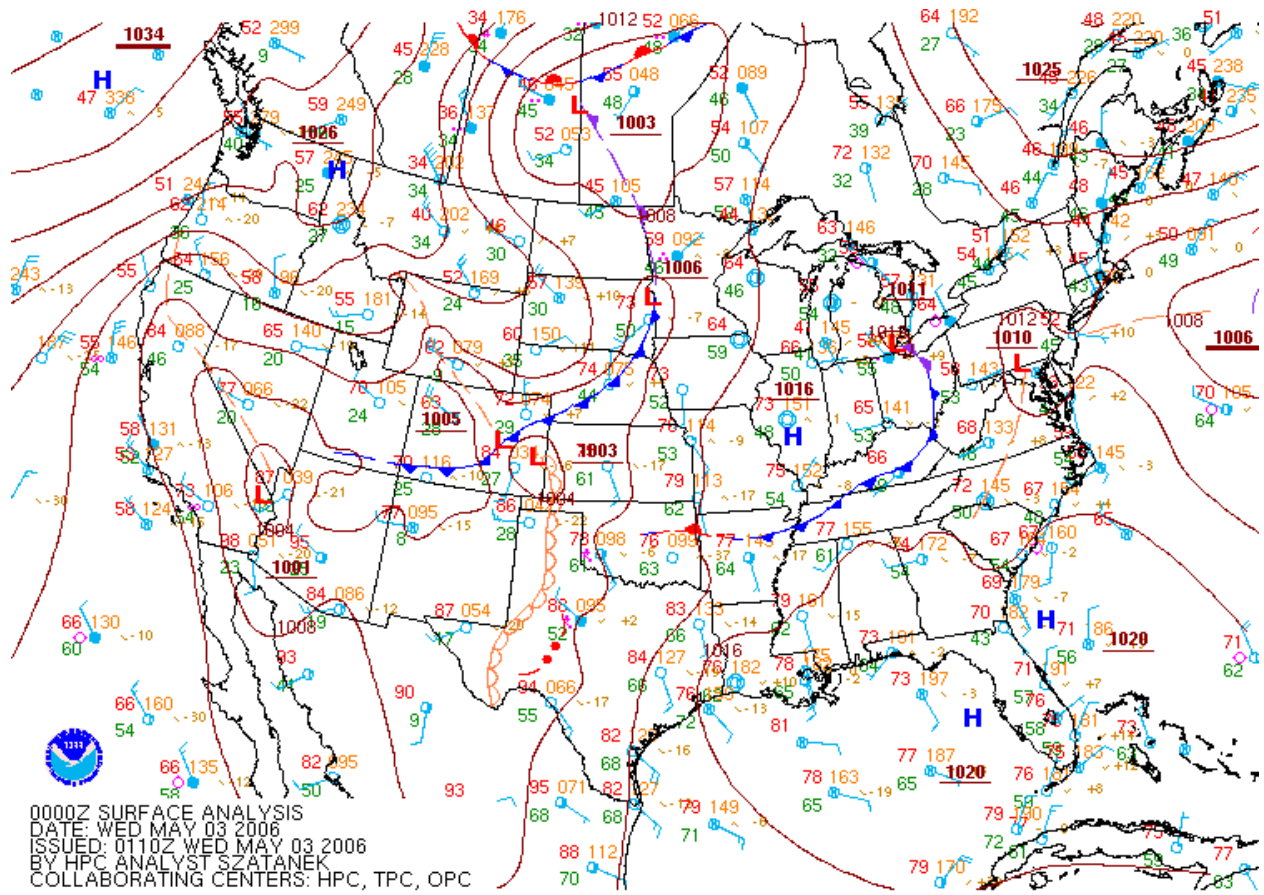


Fig. 5: Synoptic situation of the 2 May 2006 dryline.

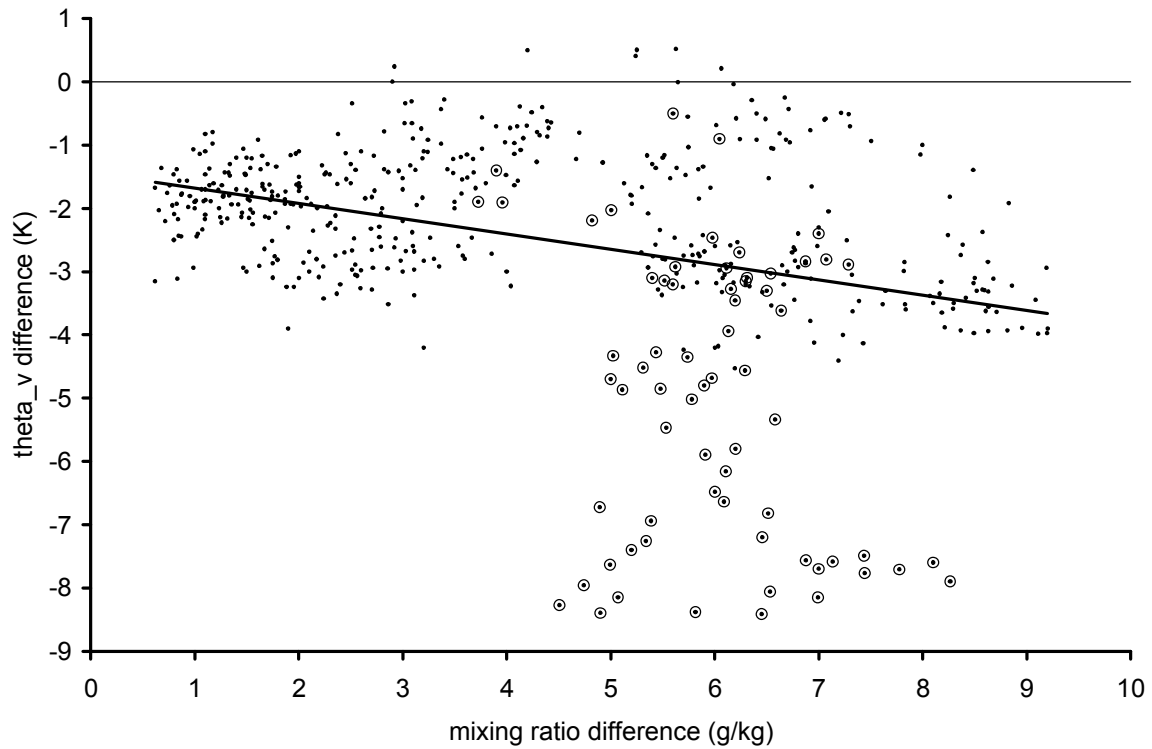


Fig. 6: Scatterplot of the difference in mixing ratio versus the difference in virtual potential temperature, between stations on opposite side of the dryline, at any time before sunset. The linear regression line is shown as well. The circled points apply to the 2 May 2006 dryline.

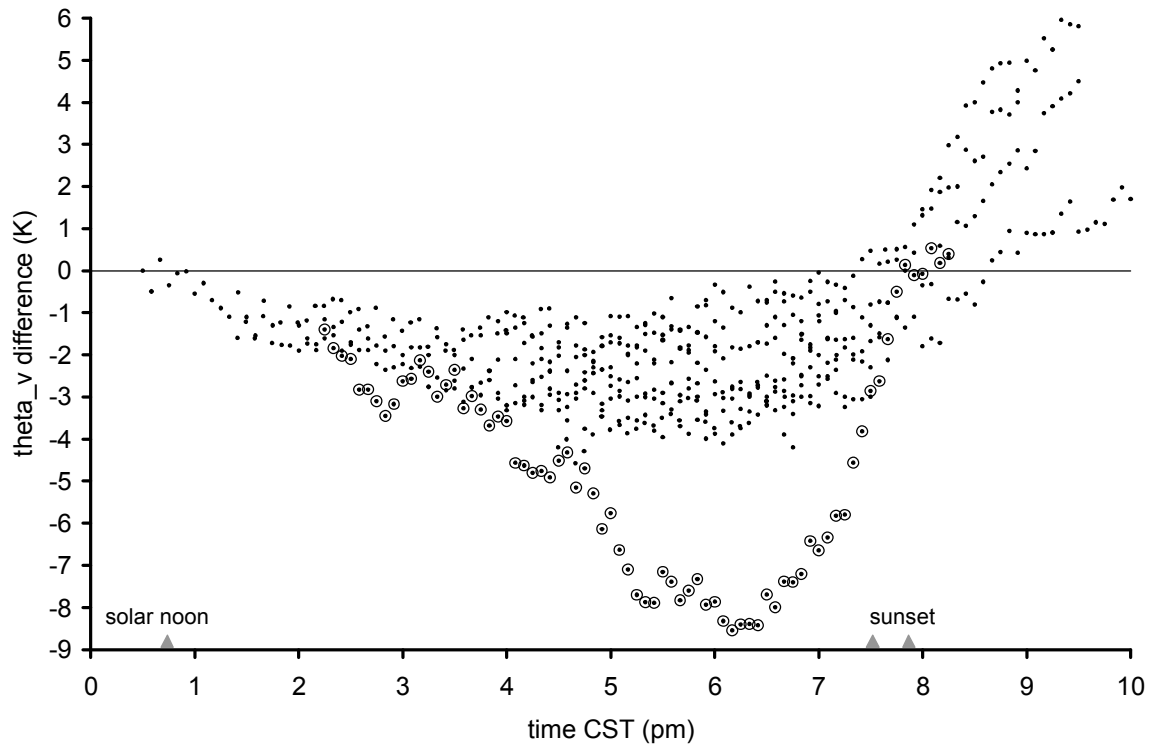


Fig. 7: Trend of $\Delta\theta$, across the drylines (CST=UTC-6). The circled points apply to the 2 May 2006 dryline. The times of solar noon and sunset (on 1 May and 31 May) in Lubbock, Texas, are indicated.

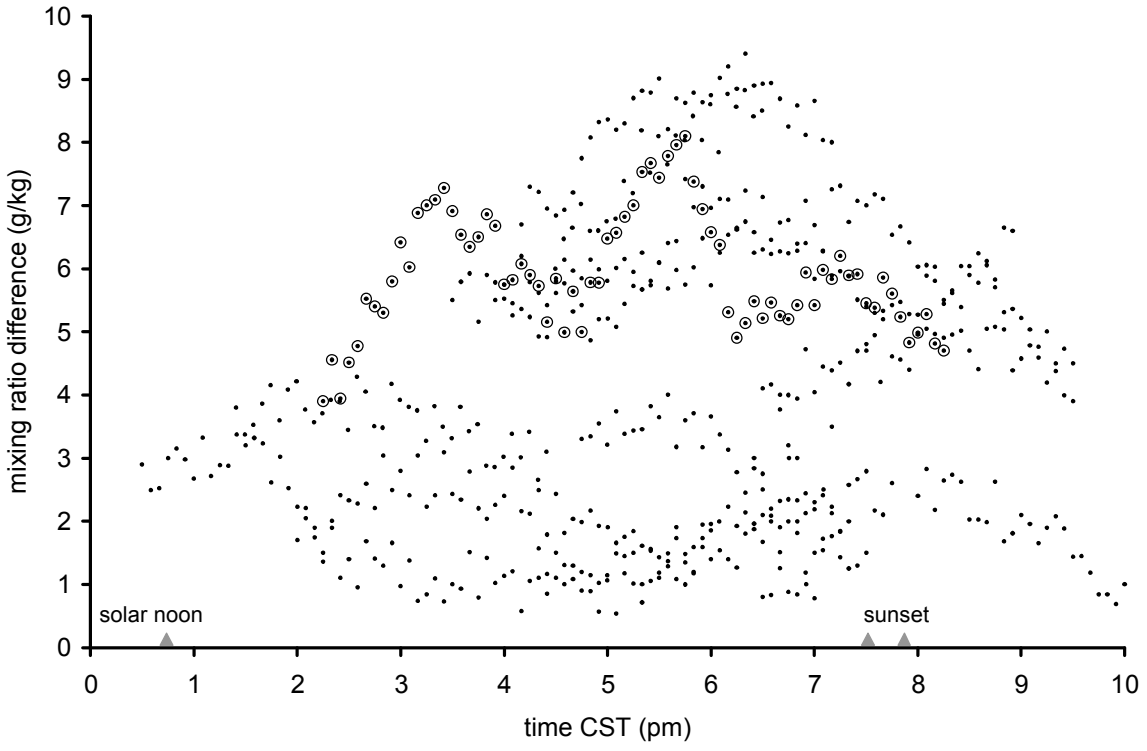


Fig. 8: As Fig. 7, but for the humidity difference Δr_v .

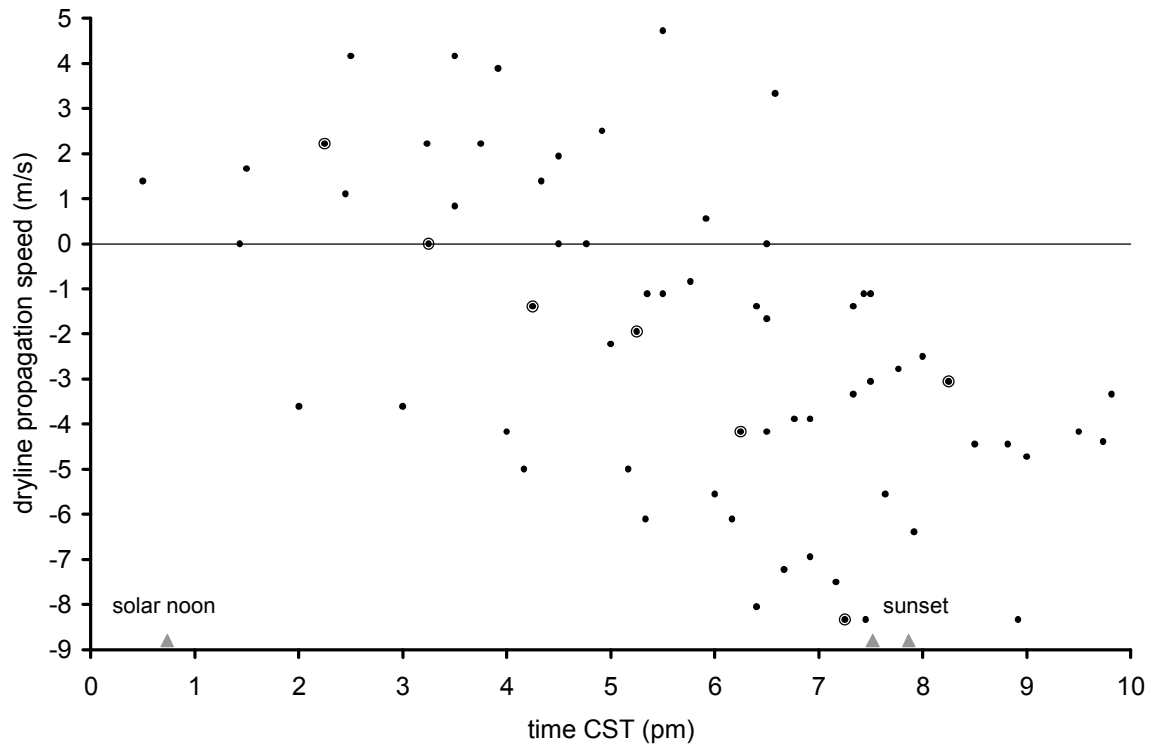


Fig. 9: Trend of the propagation speed of the dryline fine-line. The circled points apply to the 2 May 2006 dryline.

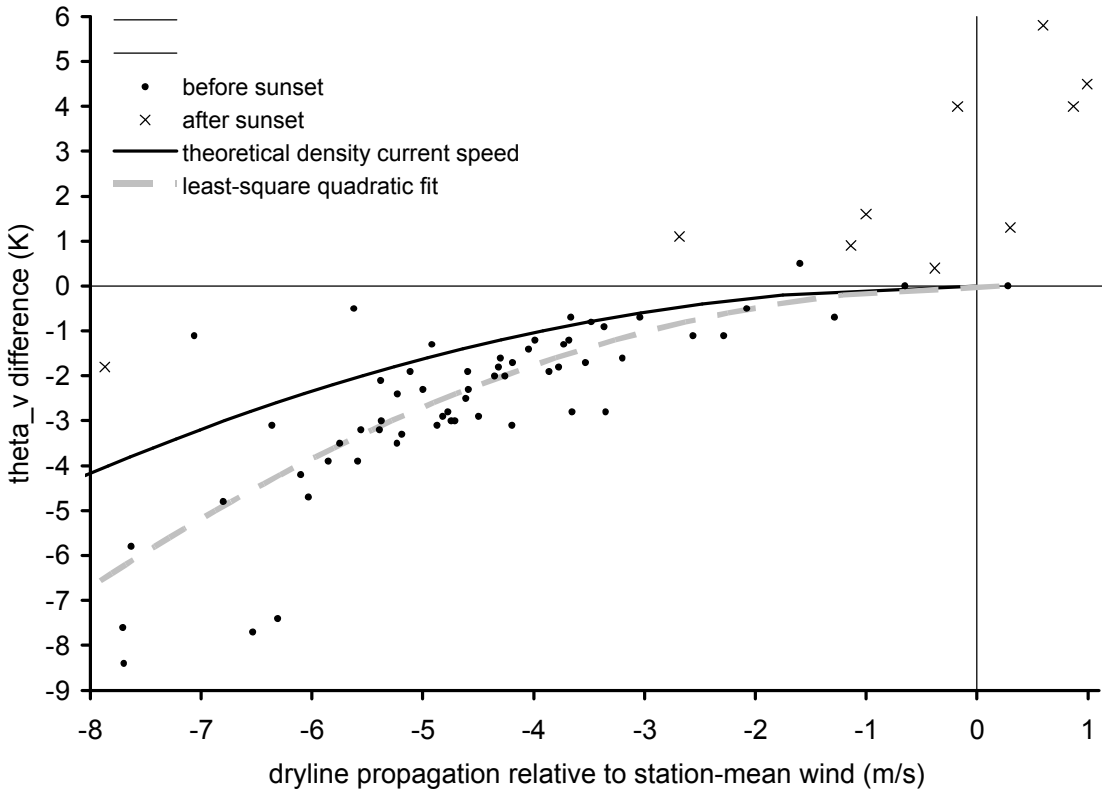


Fig. 10: Scatterplot of the dryline propagation speed relative to the ambient flow (U_{rel}) against $\Delta\theta_v$. Also shown are a theoretical dependence of density current speed on $\Delta\theta_v$, and the least-square fit for the points with $\Delta\theta_v < 0$.